Korean J. Chem. Eng., 34(3), 723-733 (2017)
DOI: 10.1007/s11814-016-0311-3

pISSN: 0256-1115
eISSN: 1975-7220

A novel hydrothermal releasing synthesis of modified SiO_2 material and its application in phenol removal process

Xinyu Yang, Xiaoyao Liu, Wenjing Tang, Yajun Gao, Huijuan Ni, and Jianbin Zhang†

College of Chemical Engineering, Inner Mongolia University of Technology, Hohhot 010051, China
(*Received 3 May 2016 • accepted 2 November 2016*)

Abstract−A modified SiO_2 material (MSM) was successfully synthesized by using Na_2SiO_3 and a novel CO_2SM in the presence of CTAB through an innovative hydrothermal releasing treatment protocol. The MSM was systemically characterized using several techniques, including N_2 adsorption-desorption isotherm, thermogravimetric analysis (TGA), Fourier transform infrared spectroscopy (FTIR), scanning electron microscopy (SEM), transmission electron microscopy (TEM) and X-ray diffraction (XRD). The CO_2SM as a platform for CO_2 capturing and releasing can be reversibly used for multiple cycles without significant loss of capabilities. The optimum conditions for the preparation of MSM were identified as follows: Na_2SiO_3 concentration, 0.2 mol/L; hydrothermal temperature, 120 °C; CO_2SM dosage, 6 g; CTAB concentration, 24 g/L, reaction time, 12 h. Additionally, the MSM exhibited high efficiency for the removal of phenol from aqueous solution: it showed a phenol adsorption capacity of 91.29 mg/g when shaken with the aqueous phenol solution at 180 rpm for 1 h at 25 °C.

Keywords: MSM, CO_2SM, Hydrothermal Releasing Method, Adsorption, Phenol

INTRODUCTION

Porous silica materials have been made via acid treatment [1-5] of various silica sources, such as tetraethyl orthosilicate, phenytriethoxysilane, notyltrimethoxysilane, and propyltrimethoxysilane [6-8]. However, this method suffers from various shortcomings, including costly raw materials, generation of secondary pollutants, and difficulty in large-scale industrial production. In contrast, hydrothermal methods have been extensively utilized to fabricate silica-related micro- and nanomaterials [9-21]. In particular, hydrothermal synthesis is amenable to treatments of mesoporous silica during and after the reaction, and it thus gives products that are superior in thermal stability, mesoscopic regularity, and structural porosity [15-17]. Although hydrothermal methods have been applied extensively, the existing literature contains relatively few systematic studies on the silica chemistry under hydrothermal conditions [16,19]. In this work, a novel and recyclable CO_2 storage material (CO_2SM) was used as a raw material to synthesize the MSM via an innovative hydrothermal releasing protocol employing cetyltrimethyl-ammonium bromide (CTAB) as a surfactant. The CO_2SM [22] was readily prepared in the medium of EDA+TEG under mild conditions, and it exhibited remarkable CO_2 capturing and releasing capabilities over multiple cycles [23,24]. CTAB is generally used to fabricate porous materials. Unger's group [25] successfully prepared ordered mesoporous silica spheres in the same synthesis system as that of silica spheres by introducing C_{16}TAB as template in 1997. Yoo et al. [26] used CTAB as a surfactant after hydrothermal transformations; pseudomorphic products of parent silica spheres synthesized in ethanol ($HTSiO_2$-EtOH) are mesoporous throughout and have smooth surfaces. Zhang group [27] successfully fabricated HMSs through directed surface sol-gel process of TEOS on the template of core shell microspheres of polystyrene-co-poly(4-vinylpyridine) (PS-co-P4VP) in the presence of C_{16}TAB in neutral aqueous solution at room temperature. Accordingly, our hydrothermal releasing method is based on CTAB as a surfactant. In our previous work, we reported the SiO_3^{2-} leaching method that made use of coal slag and coal gangue to recover silicon raw materials from waste resources [28,29]. However, because the composition of the SiO_3^{2-} leaching solution is complex, in this work the MSM was synthesized using Na_2SiO_3 as the raw material.

Phenolic compounds are almost ubiquitous pollutants due to their widespread occurrence in industrial wastewater [30], and they can cause severe damage to environment and organisms because of their high toxicity [31-33]. Therefore, it is imperative to remove phenolic compounds from industrial wastewater. Several conventional methods are often employed for the removal, including chemical precipitation, sorption, membrane processes, reverse osmosis, electrolytic recovery, and liquid-liquid extraction [34,35]. Unfortunately, these processes are costly in treating secondary toxic sludge, and can become ineffective when the pollutants exist in wastewater at low concentration [36]. In contrast, adsorption is an efficient and simple method to treat wastewater. For example, Li [37] utilized graphene as an adsorbent to remove phenol, and reported an adsorption capacity of 53.19 mg/g. Similarly, Chen [38] prepared PEI@SiO_2 to adsorb phenol, and Sean [39] synthesized zeolite and mesoporous silica nanomaterials to purge environmental pollutants. However, the abovementioned adsorbents are difficult to synthesize, costly in feedstock, and not fully satisfactory in adsorption capacity.

In this work, through a novel hydrothermal releasing method, the MSM was prepared from the CO_2SM and Na_2SiO_3 in the pres-

†To whom correspondence should be addressed.
E-mail: tadzhang@pku.edu.cn

ence of CTAB. The obtained MSM was characterized by TGA, FTIR, SEM, XRD, TEM, and N_2 adsorption-desorption isotherm, and its adsorption performance was assessed in aqueous solutions containing phenol. Several operating factors were systemically investigated, including initial phenol concentration, dosage of adsorbent, pH value of the solution, and temperature, to determine how they affected the adsorption.

EXPERIMENTAL

1. Material

Na_2SiO_3 and cetyltrimethyl ammonium bromide (CTAB) were purchased from Tianjin Wind Ship Chemical Technology Co., Ltd. Synthesis method and detail information of CO_2SM refer to our previous work [40]. Phenol with a purity of more than 99.0 wt% was purchased from Tokyo Chemical Industry Co., Ltd. All other reagents used were analytical grade and were used without further purification.

2. Hydrothermal Preparation of the MSM

The MSM was prepared by the hydrothermal releasing method. Schematic representation for the MSM and adsorption of phenol is shown in Fig. 1.

Typically, 25 mL Na_2SiO_3 solution (0.2 M) was pipetted into a vial, and then 0.6 g of CTAB was dissolved into the Na_2SiO_3 solution. After that, 6 g CO_2SM powder was transferred into a 100 mL Teflon-lined autoclave. Finally, the autoclave was kept at 120 °C for 6-36 h. White powder was obtained after reaction and washed several times with deionized water and ethanol. The ultimate MSM was dried at 100 °C overnight and ground into power for adsorption of phenol.

In this process, the optimum MSM preparing conditions, including dosage of CO_2SM, the mass concentration of the CTAB, hydrothermal temperature and reaction time, and the properties of the final products, were also systematically studied.

3. Characterization

The phase structure of MSM and crystallinity of the sample were checked by XRD analysis (Shimadzu, D/max-2200/PC) with Cu K_α radiation operated at 40 kV and 40 mA. The phase transition characteristics and functional groups of the samples were determined through FTIR technology, using the KBr pellet technique (Nicolet, Nexus 670), in the frequency region of 4,000 to 400 cm^{-1}. The microstructure and morphology of sample was analyzed by SEM analysis (HITACHI, S-3400N) with an energy dispersive X-ray spectrometer (EDS). TEM analysis was by using a JEOL JEM-2100F field emission electron microscope with an acceleration voltage of 200 kV. The BET specific surface areas of the samples were calculated by N_2 adsorption isotherms obtained from a Quadrasorb SI-MP analyzer at 77 K. All the samples were degassed under vacuum at 300 °C for 3 h before testing. The pore size distributions in the adsorption branches of the isotherms were obtained by using the Barret-Joyner-Halenda (BJH) method. The pore size and total volume were calculated based on pore size distribution curves. The thermal stability of the sample was determined by thermogravimetry and differential thermogravimetry (TG-DTG) analysis by using an NETZSCH STA 409 PC/PG at a heating rate of 10 K/min.

4. Adsorption Test

The adsorption experiments of phenol were carried out in 150 mL conical flasks. In a typical experiment, 0.2 g of the MSM was added to 50 mL of phenol solution. These flasks were sealed to avoid

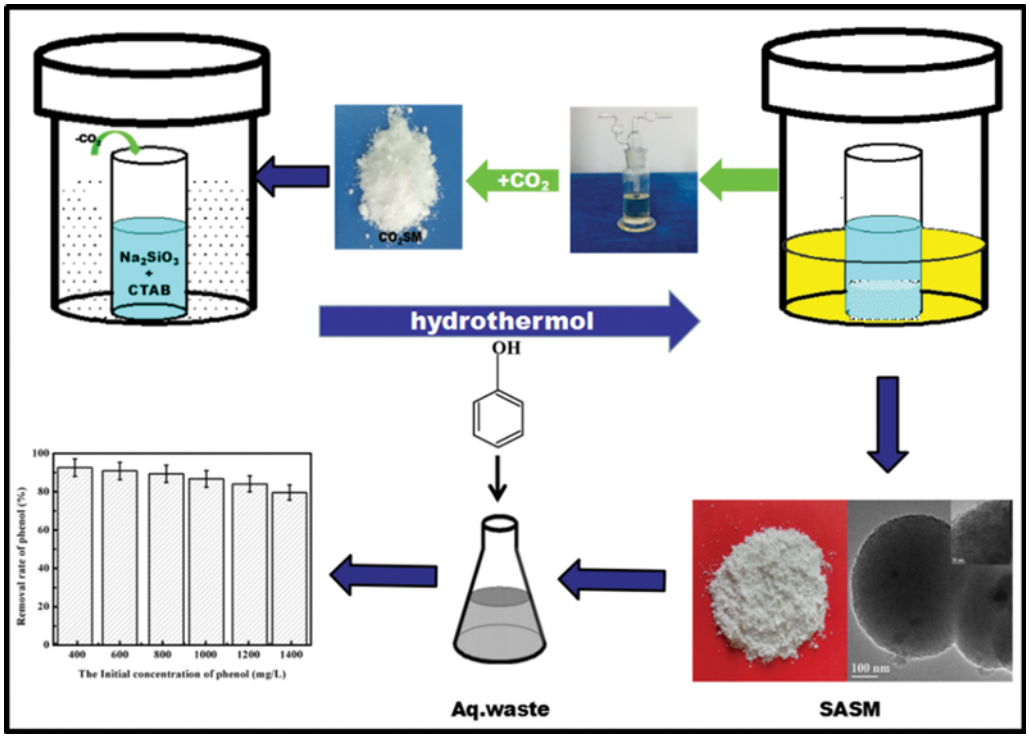

Fig. 1. Schematic representation for the MSM and adsorption of phenol.

evaporation, and then were shaken in an oscillation incubator at 170 rpm. This allowed the solution to equilibrate and to arrive at practically the same uptake condition in every run. The concentration of phenol was then measured through the 4-aminoantipyrine procedure [41] by a TU-1810 UV-V spectrophotometer. In the batch mode, the stock NH_4Cl-NH_4OH buffer solution (0.5 mL) was added to the phenol solution (50.0 mL) pending assay. The pH of the solution was adjusted to 10.0 using the NH_4Cl-NH_4OH buffer solution, and 4-aminoantipyrine solution (1.0 mL) and potassium ferricyanide solution (1.0 mL) were then added. The resultant mixture was shaken thoroughly and allowed to equilibrate for 10 min. Absorbance of the resultant solution was then measured using the spectrophotometer at 510 nm.

5. Models

5-1. Equilibrium Modeling Study

Langmuir and Freundlich isotherm models were used to investigate the adsorption equilibrium between the solution phase and the MSM phase. The linear form of Langmuir isotherm equation [42] was represented by the following equation:

$$\frac{1}{q_e}=\frac{1}{q_{max}K_L}\times\frac{1}{C_e}+\frac{1}{q_{max}} \quad (1)$$

The linearized Freundlich isotherm equation [43], which was based on adsorption on heterogeneous surface and active sites with different energy [44], was represented by the following equation [45]:

$$\log q_e=\log K_F+\frac{1}{n}\log C_e \quad (2)$$

5-2. Thermodynamic Modeling Study

Temperature dependence of adsorption process was associated with several thermodynamic parameters, which were necessary to determine whether the process was spontaneous or not. Gibbs free energy change (ΔG^o) of the adsorption process could be determined from the following equation:

$$\Delta G^o=-RT\ln K_e \quad (3)$$

The K_e value was calculated using the following equation:

$$K_e=q_e/C_e \quad (4)$$

Relation among ΔG^o, enthalpy change (ΔH^o) and entropy change (ΔS^o) could be expressed by the following equation:

$$\Delta G^o=\Delta H^o-T\Delta S^o \quad (5)$$

Eq. (5) could be written as:

$$\ln K_e=-\frac{\Delta G^o}{RT}=-\frac{\Delta H^o}{RT}+\frac{\Delta S^o}{R} \quad (6)$$

According to Eq. (6), ΔH^o and ΔS^o values could be calculated from the slope and intercept of the plot of in K_e versus 1/T, respectively [46-49].

RESULTS AND DISCUSSION

1. Effect of Preparation Conditions on the MSM

Based on the experimental results, Na_2SiO_3 can react with CO_2 released from the CO_2SM at high temperature to form SiO_2 according to the reaction represented by Eqs. (7)-(8). Furthermore, to obtain the maximum adsorption capacity of MSM, we systematically investigated various preparation conditions, including Na_2SiO_3 concentration, CO_2SM dosage, the concentration of CTAB, hydrothermal temperature T, and reaction time t.

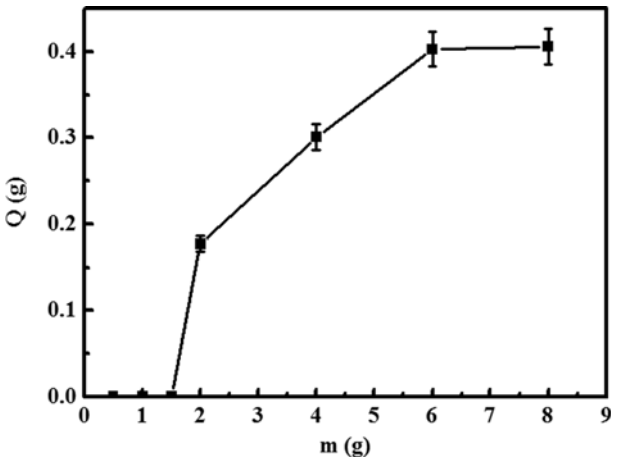

Fig. 2. Effect of CO_2SM dosage on the yield of the porous MSM.

The main chemical reactions occurred in the hydrothermal releasing processes were as follows:

$$SiO_3^{2-}+CO_2(\text{Little})+nH_2O=CO_3^{2-}+SiO_2\ nH_2O\downarrow \quad (7)$$

$$SiO_3^{2-}+2CO_2(\text{excess})+(n+1)H_2O=2HCO_3^-+SiO_2\ nH_2O\downarrow \quad (8)$$

1-1. Effect of CO_2SM Dosage on the Yield of the MSM

A set of initial values were selected for the following variables, T =100 °C, t=12 h, 0.2 M Na_2SiO_3 and without surfactant, to study the effect of CO_2SM dosage on the yield of MSM. According to Eq. (7) and Eq. (8), low MSM yields were obtained at low concentrations of Na_2SiO_3. Consequently, a higher concentration of the Na_2SiO_3 solution was employed to ensure the synthesis was as complete as possible. Based on these results, the optimal concentration of the Na_2SiO_3 solution was determined to be 0.2 M.

As shown in Fig. 2, when the dosage of CO_2SM increased from 1 to 6 g, the yield of MSM improved considerably from 0 to 0.4031 g. However, after the dosage of CO_2SM reached 8 g, the MSM yield did not increase further, which was in accord with Eq. (7) and Eq. (8) and subject to conservation of mass. When 6 g CO_2SM was used, the CO_2 released from the CO_2SM reacted completely with Na_2SiO_3 (reaction 8). Since the yield of MSM remained stagnant at higher CO_2SM dosage, to use more than 6 g CO_2SM was not necessary and only led to excessive material consumption.

Unfortunately, the product hence prepared exhibited minimal adsorption capacity for phenol. Therefore, in the following investigations, CTAB was employed as a surfactant in preparing the MSM.

1-2. Effect of CTAB Concentration on the Adsorption Capacity of MSM

We next optimized the phenol adsorption capacity of the MSM by using CTAB in the hydrothermal synthesis. The MSM was prepared through hydrothermal reaction at 100 °C for 12 h using 6 g CO_2SM and 0.2 M Na_2SiO_3 in the presence of varying amounts of CTAB (i.e., 1.5, 4.4, 7.3, 10.9, 16, 24, 40, 64, and 80 g/L). Fig. 3 shows

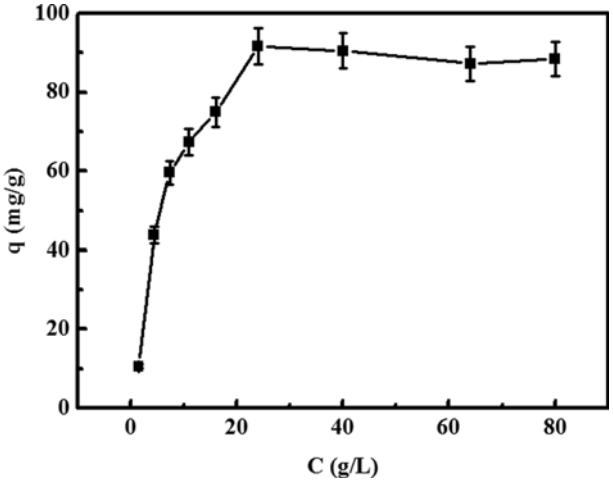

Fig. 3. Effect of CTAB concentration on the adsorption capacity of the porous MSM.

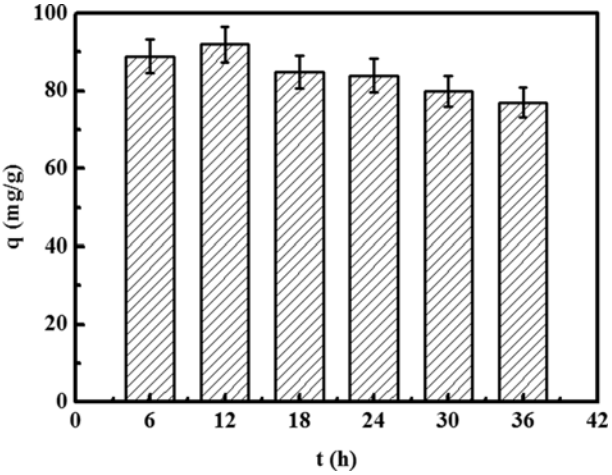

Fig. 5. Effect of preparation time on the adsorption capacity of the MSM.

the effect of CTAB concentration on the phenol adsorption capacity of the MSM.

Fig. 3 shows that the adsorption capacity of MSM increased sharply to 91.82 mg/g when the use of CTAB increased up to 24 g/L. However, a slight decrease in the adsorption capability was observed in the concentration range of 24 g/L to 80 g/L. Thus, it is reasonable to set the concentration of CTAB at 24 g/L to avoid excessive material consumption.

1-3. Effect of Hydrothermal Temperature on the Adsorption Capacity of MSM

The effect of preparation temperature on the adsorption capacity of MSM was studied at the Na_2SiO_3 concentration of 0.2 M, t= 12 h, the CO_2SM dosage of 6 g, and the CTAB concentration of 24 g/L. Fig. 4 unambiguously displays that the maximum adsorption capacity of MSM was obtained at the hydrothermal temperature of 120 °C. At 120 °C, CO_2 was slowly released from the CO_2SM and could react completely with Na_2SiO_3. When the temperature exceeded 120 °C, CO_2 was released too quickly. The resulting MSM product was precipitated spontaneously and its molecules were compactly arranged, which significantly reduced the surface area and adsorption capability. Hence, the optimum hydrothermal temperature was determined to be 120 °C.

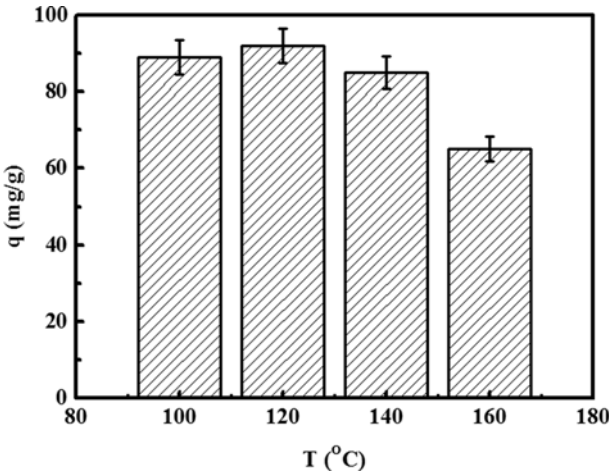

Fig. 4. Effect of hydrothermal temperature on the adsorption capacity of the MSM.

1-4. Effect of Preparation Time on the Adsorption Capacity of MSM

The effect of preparation time on the adsorption capacity of MSM was examined at the concentration of 0.2 M Na_2SiO_3, T= 120 °C, the CO_2SM dosage of 6 g, and the CTAB concentration of 24 g/L. Fig. 5 clearly illustrates that the maximum adsorption capacity of the MSM was obtained at the hydrothermal time of 12 h. When the preparation time was less than 12 h, the CO_2 released from the CO_2SM was insufficient for the reaction to complete. Fig. 5 shows that the optimum reaction time was 12 h.

Therefore, the optimum preparation conditions of MSM were determined to be as follows: the Na_2SiO_3 concentration of 0.2 M, the CO_2SM dosage of 6 g, the CTAB concentration of 24 g/L, the hydrothermal temperature of 120 °C, and the hydrothermal time of 12 h.

2. Orthogonal Experiments of MSM Preparation Conditions

We designed a set of orthogonal experiments (DOE) to determine the relative impact of each factor on the adsorption capability of MSM under the optimum preparation conditions. The orthogonal experiments shown in Table 1 were utilized to reduce the numbers of experiment and to reveal more information. The results of orthogonal experiments are shown in Table 2.

As shown in Table 2, the order of major three factors is: B (reaction time)>A (C_{CTAB})>C (temperature). The optimal combination is $A_1B_1C_1$, which represents reaction temperature at 120 °C, reaction time of 12 h, and CTAB concentration (C_{CTAB}) of 24 g/L. This

Table 1. Factors and levels of orthogonal experiments

Factors	A (C_{CTAB}) (g/L)	B (Reaction time) (h)	C (Temperature) (°C)
1	24	12	120
2	16	6	100
3	40	18	140

Table 2. The results of orthogonal experiments

Num.	Factors			Adsorption capacity of MSM (mg/g)
	A	B	C	
1	1	1	1	91.29
2	1	2	2	88.14
3	1	3	3	87.67
4	2	1	2	86.51
5	2	2	3	80.79
6	2	3	1	89.21
7	3	1	3	88.57
8	3	2	1	86.27
9	3	3	2	83.80
K_1	267.1	266.43	266.77	
K_2	256.51	255.2	258.45	
K_3	258.64	260.68	257.03	
k_1	89.03	88.81	88.92	
k_2	85.50	85.07	86.15	
k_3	86.21	86.89	85.68	
R	3.53	3.74	3.24	
Order		B>A>C		
Optimal level	A_1	B_1	C_1	
Optimal group		A_1 B_1 C_1		

agrees with previous results from one-factor-at-a-time (OFAT) experiments.

3. Characterization of the MSM

3-1. FTIR Analysis

Fig. 6 shows the FTIR spectrum of the MSM. The bands at 459 cm^{-1}, 783 cm^{-1}, and 1,065 cm^{-1} were assigned to the bending vibration of Si-O-Si [50], characteristic absorption of SiO_3^{2-}, and antisymmetric stretching vibration of Si-OH [51], respectively. In addition, the absorption bands at 2,925 cm^{-1} and 2,848 cm^{-1} were attributed to -CH_2- stretching vibrations [52]. The absorption bands at 3,442 cm^{-1} and 1,627 cm^{-1} corresponded to the O-H antisymmetric stretching vibration and H-O-H bending mode of the water molecule [53], respectively, which indicated that adsorbed water and crystal water existed in the material MSM.

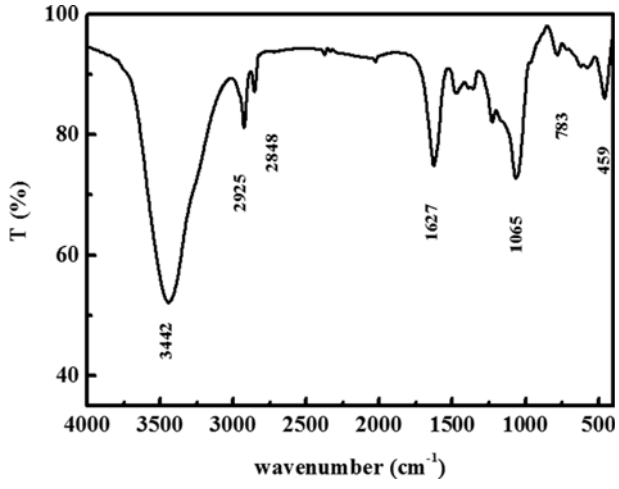

Fig. 6. FTIR spectrum of the MSM.

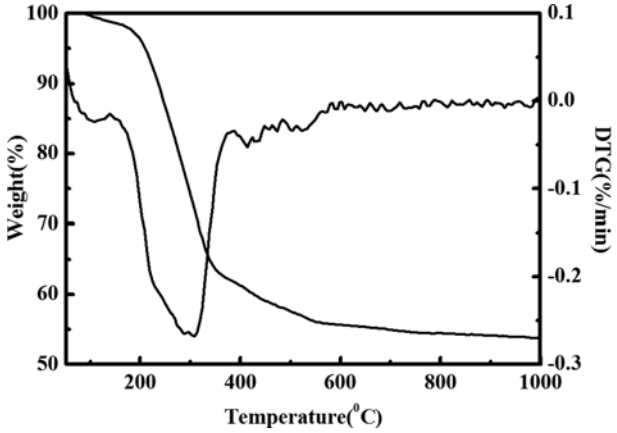

Fig. 7. TGA curve of the MSM.

3-2. Thermogravimetric Analysis

The thermal stability of the MSM was assessed using thermal gravimetric analysis (TGA) analysis under a nitrogen atmosphere, and the results are displayed in Fig. 7. Thermal decomposition of the MSM was carried out at a heating rate of 10 K·min^{-1} in the temperature range of 30 °C to 1,400 °C. A total mass loss of 0.584 mg was observed, which accounted for 51.73 wt% of the total weight.

As shown in the TGA of MSM (Fig. 7), the pyrolysis process can be divided into three stages. The first stage in the range of 35-180 °C corresponds to the removal of physically absorbed water and interlayer water [54]. The second stage in the range of 180-295 °C represents removal of the organic groups in the material [55]. According to the literature [56-58], the decomposition of alkyl groups should occur at 473-573 K. In this temperature range, the MSM exhibited a 30.38% weight loss. In the third stage between 295-621 °C, the mass loss was attributed to the dehydration of the material [59].

3-3. XRD Analysis

Fig. S1 shows the XRD pattern of MSM. The XRD pattern of

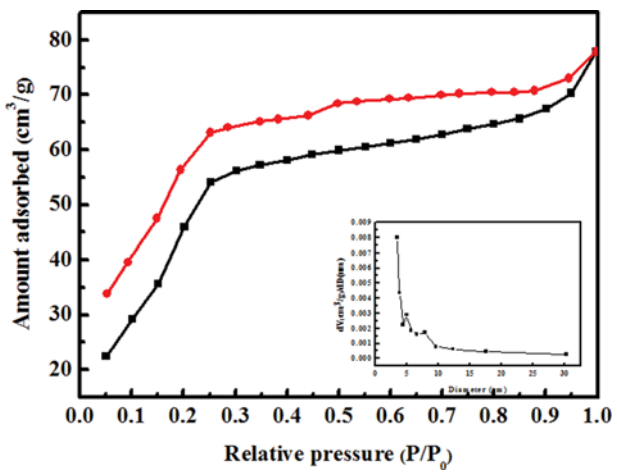

Fig. 8. N_2 adsorption-desorption isotherm at 77 K and the BJH adsorption pore size distribution (inset) of the MSM.

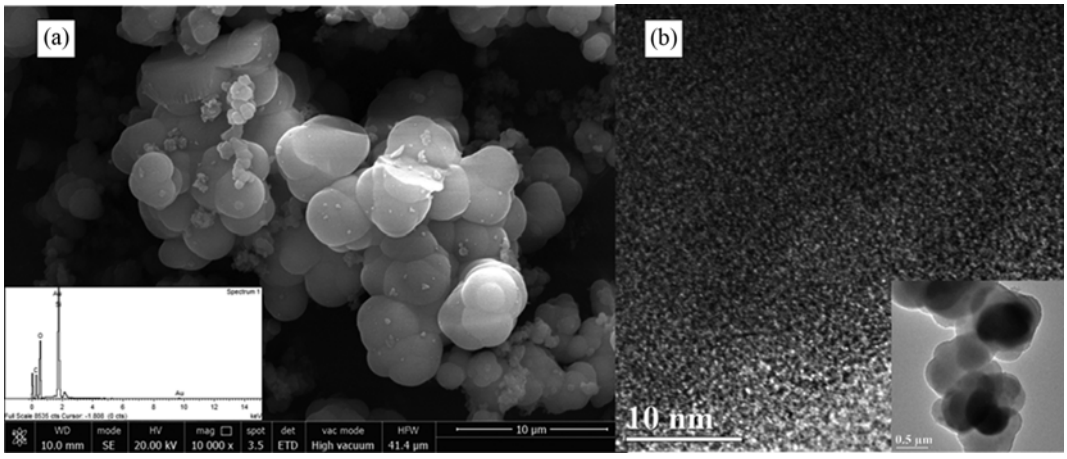

Fig. 9. TEM and SEM images and the energy spectrum (inset) of the MSM.

MSM shows a broad diffraction peak in the range of 2θ=15-30 °, indicating that MSM mainly has amorphous silica structure [60-62], consistent with the results of SEM.

3-4. N_2 Adsorption-desorption Isotherm Analysis

The N_2 adsorption-desorption isotherm is shown in Fig. 8, and the pore size distribution determined by BJH analysis from the adsorption branch of the N_2 adsorption isotherm is depicted in the inset image.

As shown in Fig. 8, the MSM seems to have a combination of type-I and type-II isotherms, and is hence an irregular mesoporous material. The pore diameter of the materials was centered between 3 to 30 nm, and the average pore diameter, calculated by using the BJH method, was 3.412 nm. The BET specific surface area and the pore volume of the material are calculated from the isotherm to be 14.43 $m^2 \cdot g^{-1}$ and 0.038 $cm^3 \cdot g^{-1}$, respectively.

3-5. SEM and TEM Analysis

Representative SEM and TEM images of the MSM are presented in Fig. 9. As can be seen in Fig. 9(a), the SEM image revels that the prepared MSM was 100-500 nm in size and had a stack-up irregular spherical structure. As shown in Fig. 9Aa of energy spectrum (inset), the surface of the MSM predominantly consisted of C, O and Si. The distribution of the particle size and morphology of the prepared materials could be directly observed through TEM characterization, which showed massive narrow channels and represented irregular mesoporous structure (Fig. 9(b)). Possible synthesis mechanism is explained as follows:

$$nH_2NCH_2CH_2NH_2 + nHOC_2H_4OC_2H_4OC_2H_4OH \underset{\Delta}{\overset{CO_2}{\rightleftharpoons}} [H_3\overset{\oplus}{N}CH_2CH_2\overset{\oplus}{N}H_3\ \overset{\ominus}{O}\text{-}\overset{O}{\overset{\|}{C}}\text{-}O\text{-}C_2H_4OC_2H_4OC_2H_4\text{-}O\text{-}\overset{O}{\overset{\|}{C}}\text{-}\overset{\ominus}{O}]_n \quad (9)$$

$$SiO_3^{2-} + CO_2(\text{Little}) + nH_2O = CO_3^{2-} + SiO_2\ nH_2O\downarrow \quad (10)$$

$$SiO_3^{2-} + 2CO_2(\text{excess}) + (n+1)H_2O = 2HCO_3^- + SiO_2\ nH_2O\downarrow \quad (11)$$

In this study, the water medium contributed to the transformation of Na_2SiO_3 into SiO_2 and CTAB was added as surfactant. In our previous work [22], we reported solid CO_2-storage materials (CO_2SMs) could be employed as an effective CO_2 capturing/releasing platform in detail. The CO_2 released from the solid CO_2-storage materials (CO_2SM) under higher temperature and the system of EDA+TEG exhibits remarkable CO_2 capturing and releasing capabilities for multiple cycles that can be recycled to offer CO_2 for Eqs. (10)-(11) consistently.

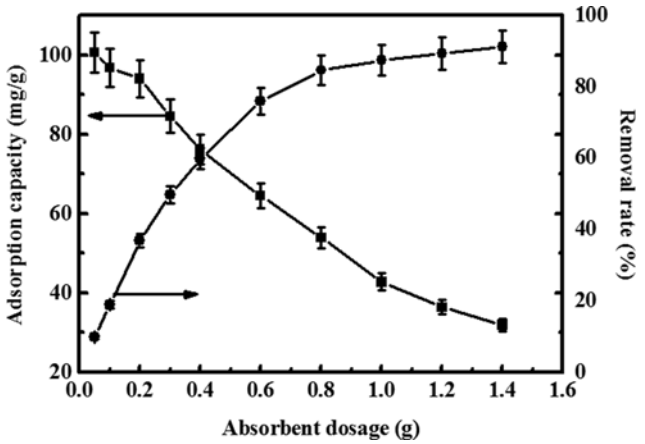

Fig. 10. Effect of adsorbent dose on the adsorption of phenol.

4. The Adsorption test of MSM

A series of batch adsorption experiments were conducted to assess the adsorption behavior of the MSM.

4-1. Effect of Adsorbent Dosage on the Removal of Phenol

The effect of adsorbent dosage on the removal of phenol (Fig. 10) was evaluated in 1,000 mg/L phenol aqueous solutions and at T_0=25.0 °C. It showed that the removal rate of phenol was increased with increasing dosage of adsorbent. In the aqueous solution of phenol (1,000 mg/L), the rate of phenol removal arrived at a plateau when the dosage of the MSM adsorbent exceeded 16 g/L. This is because the exchange equilibrium was reached between phenol in aqueous solution and phenol adsorbed on the MSM [63].

4-2. Effect of Reaction Time and Temperature

The phenol adsorption capacity of MSM increased dramatically at the initial period of approximately 5 min. This phenomenon is because large numbers of vacant sites are available during the initial period. After that, the remaining vacant sites are difficult to be

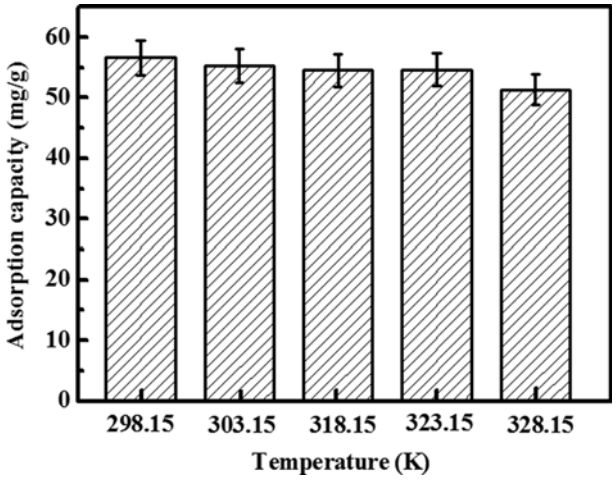

Fig. 11. Effect of reaction contact time and temperature.

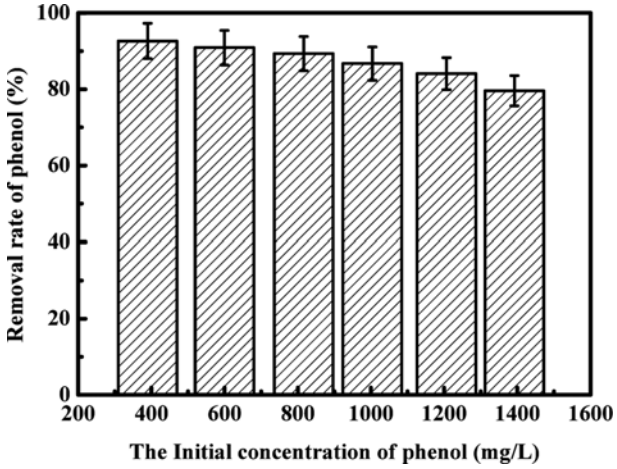

Fig. 13. Effect of the initial concentration on the adsorption of phenol.

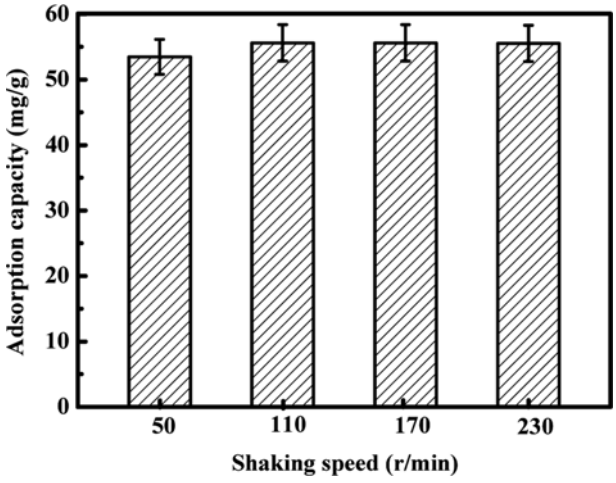

Fig. 12. Effect of the shaking speed on the adsorption of phenol.

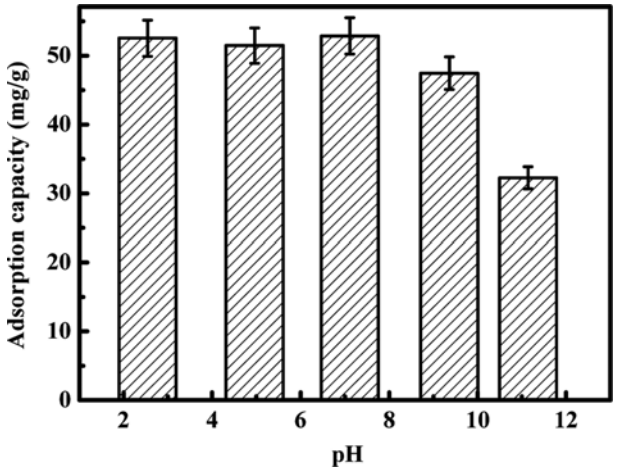

Fig. 14. Effect of pH on the adsorption of phenol.

occupied by the phenol molecules due to the repulsive forces between the adsorbed solute molecules on the surface and solute in solution phase.

Fig. 11 shows that the adsorption capacity of MSM decreased slightly from 56.64 mg/g to 51.34 mg/g when temperature was increased from 25 °C to 45 °C. This is because the adsorbate tends to escape from the solid phase into the solution when the adsorption is exothermic [61].

4-3. Effect of the Shaking Speed

To investigate the effect of shaking speed of shaker on the adsorption of phenol, we carried out a series of experiments with various shaking speeds in 1,000 mg/L phenol aqueous solution and at T_0=25.0 °C. The results are shown in Fig. 12.

It was found that the shaking speed directly affected the removal rate of phenol. Fig. 12 shows that the rate of phenol removal increased with rising shaking speed, which is a typical characteristic of outer diffusion [65]. To obtain a relatively higher phenol removal rate and escape excessive energy consumption, we chose the shaking speed of 170 r/min for the following investigations.

4-4. The Adsorbent on the Removal Rate of Phenol with Various Concentrations

Fig. 13 shows the effect of the MSM adsorbent on the removal rate of phenol. The removal rate of phenol at C_0=400 mg/L, 600 mg/L, 800 mg/L, 1,000 mg/L, 1,200 mg/L, and 1,400 mg/L and T_0= 25.0 °C were found to be 92.63%, 90.90%, 89.36%, 86.72%, 84.10%, and 79.62%, respectively. Apparently, the removal rate of phenol decreased with the increase of the initial concentration of phenol.

4-5. Effect of pH Value

The effect of the pH value of solution on the adsorption of phenol was also examined in a series of acidic and alkaline solutions at T_0=25.0 °C. As shown in Fig. 14, the phenol adsorption capacity of MSM at pH=2.54, 4.96, 7.11, 9.36 was 52.55 mg/g, 51.49 mg/g, 52.90 mg/g, 47.47 mg/g and 32.26 mg/g, respectively. Fig. 15 clearly shows that the MSM attained maximum adsorption capacity at pH=7.11. In addition, the maximum desorption of phenol was achieved at pH>11. The pH value of the solution is hence critical to the adsorption of phenol onto the MSM. These results are consistent with the previous report by Özkaya, who noted that sodium hydroxide facilitated desorption of phenolic compounds [66]. Moreover, this result demonstrates that pH value of the solu-

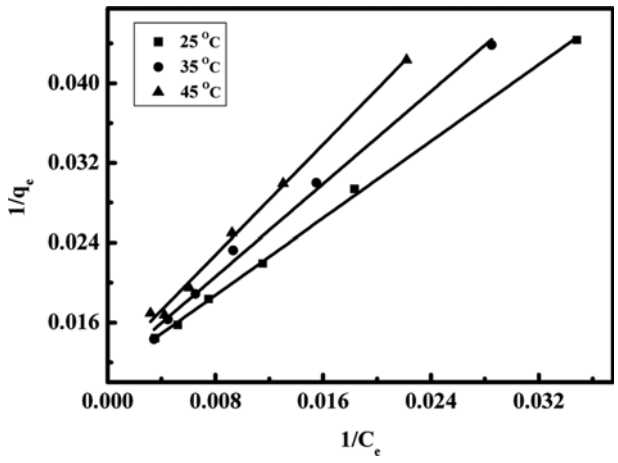

Fig. 15. Langmuir adsorption isotherm of phenol onto MSM at 25 °C, 35 °C and 45 °C.

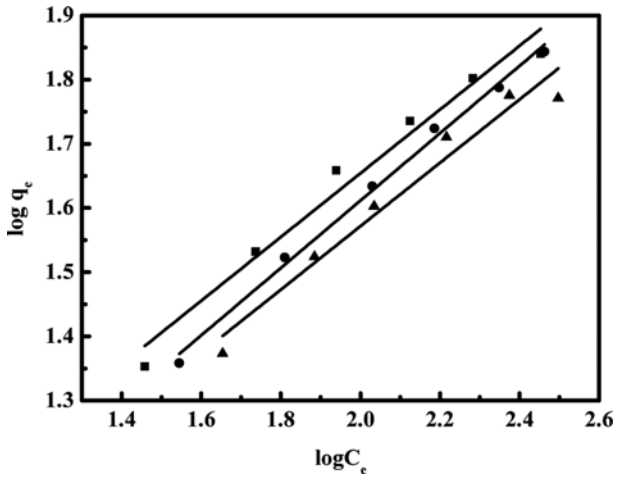

Fig. 16. Freundlich adsorption isotherm of phenol onto MSM at 25 °C, 35 °C and 45 °C.

Table 3. The comparison results on the phenol adsorption capacity of other adsorption materials

Adsorbent	Adsorption capacity (mg/g)	Reference
Activated carbon nanofibers	251.6	67
Rice husk	22	68
Graphene	53.19	69
Commercial activated carbon	49.72	70
Chemically modified green macro alga	20	71
Apricot stone shells	120	72
Modified diatomite	92	73
RCP	142.5	74
S800/A800	87/89	75
MCM-41	23	76
DTAB modified Silica	30	77
SBA	15	78
PAM	63.78	25
MSM	90.50	This work

tion is critical to the adsorption process of MSM. Table 3 summarizes the comparison results of the phenol adsorption capacity of MSM with other adsorption materials [25,67-78]. On the basis of the above results, it is evident that the MSM has a high capacity for the removal of phenol from the aqueous solution. Two different types of adsorption sites exist on the surface of MSM: less polar Si-O-Si (siloxane) groups and polar Si-OH (silanol) groups with strong hydrogen-bonding Si-OH group's interactions between them [79,80] corresponding to FTIR, which are effective for the adsorption of organic compounds due to their high adsorption energy. In addition, MSM also possesses organic groups according with vibrations at 2,925 cm^{-1} and 2,848 cm^{-1} in FTIR, which favors the organic phenolic compound adsorption on MSM [7,81].

5. Adsorption Isotherms

To investigate the mechanism of phenol adsorption on the MSM, we analyzed the experimental data by fitting them to the Langmuir and Freundlich isotherm equations. The fitting results are shown in Figs. 15 and 16. The constant parameters and correlation coefficients (R^2) are summarized in Table 4. Langmuir model is suitable for the characterizing the experimental adsorption isotherms according to the results in Table 2. It was found that the correlation coefficients at 25 °C, 35 °C, and 45 °C were 0.99875, 0.99382, and 0.99499, respectively. The Langmuir adsorption isotherm for monolayer adsorption [70] on a homogeneous surface was successfully fitted to this adsorption process, and the saturated adsorption capacity reached 90.50 mg/g. Compared with Langmuir model, the Freundlich model gave inferior fitting, and it still gave correlation coefficients of greater than 0.9 in all cases. When n= 2.0143, 1.9051 and 2.0247, their corresponding correlation coefficients were all more than 1, indicating the adsorption of phenol is a favorable process [82].

6. Adsorption Thermodynamic Studies

To further understand the adsorption process taking place between the MSM and the phenol adsorbate, we also conducted thermodynamic studies. The results are shown in Fig. 17. Thermodynamic parameters were evaluated in Table 5. The ΔG values were

Table 4. Parameters of Langmuir isotherm models at various temperature values

T (K)	Langmuir			Freundlich		
	q_m (mg/g)	b (L/mg)	R^2	K_F	n	R^2
298.15	90.50	0.0115	0.99875	4.5851	2.0143	0.96859
308.15	88.42	0.0097	0.99382	3.6461	1.9051	0.99409
318.15	85.62	0.0084	0.99499	3.8365	2.0247	0.95507

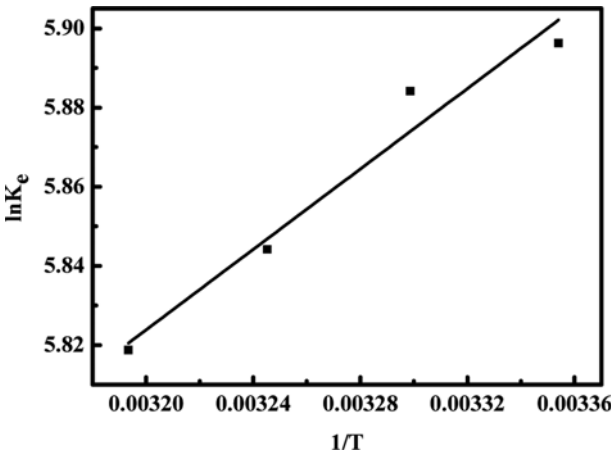

Fig. 17. Thermodynamic plot for phenol adsorption onto MSM.

Table 5. Thermodynamic parameters for the adsorption of phenol onto the MSM (p=100 kPa)

T (K)	ΔG^o (kJ/mol)	ΔH^o (kJ/mol)	ΔS^o (J/mol·K)
298.15	−14.63	−4.22	34.91
303.15	−14.83		
308.15	−14.97		
313.15	−15.15		

negative across all temperatures, implying that the adsorption was favorable and spontaneous. The adsorption of phenol onto the MSM appeared to have a negative enthalpy, which corresponds to an exothermic adsorption that decreased the uptake of phenol with rising temperature. On the other hand, the adsorption process had positive entropy [83], which was attributed to an increase in randomness at the interface between the solid and the solution and an increase in the degree of freedom of the adsorbed species [84].

CONCLUSION

A novel approach employing hydrothermal releasing treatment was successfully developed for the preparation of the MSM, which accomplished the utilization of recyclable CO_2SM through multiple CO_2 capture and release cycles. The preparation method developed herein has two remarkable features: readily available raw materials and simple process. On the basis of the results of this study, the following main conclusions can be drawn.

(1) The optimum preparation conditions of MSM were identified as follows: Na_2SiO_3 concentration, 0.2 M; CO_2SM dosage, 6 g; CTAB concentration, 24 g/L; hydrothermal temperature, 120 °C; and reaction time, 12 h.

(2) The MSM was mainly comprised of three elements: Si, O and C. Some adsorbed water and crystal water were also detected. Specifically, the adsorption capacity of SiO_2 towards phenol was 100.76 mg·g^{-1} under the following conditions: temperature, 25.0 °C; phenol solution concentration, 1,000 mg/L; MSM dosage, 10 g/L; and shaking speed, 170 rpm.

The adsorption process of phenol on MSM occurred on a homogeneous surface through a monolayer adsorption mechanism. The calculated thermodynamic parameters, including ΔG^o, ΔH^o, and ΔS^o, confirmed that the adsorption process of phenol on MSM is a favorable, spontaneous and exothermic adsorption, which is consistent with the experimental results of thermodynamic investigations.

ACKNOWLEDGEMENTS

This work was supported by the National Natural Science Foundation of China (21466028), the Program for Grassland Excellent Talents of Inner Mongolia Autonomous Region, Program for New Century Excellent Talents in University (NCET-12-1017), and training plan of academic backbone in youth of Inner Mongolia University of Technology.

SUPPORTING INFORMATION

Additional information as noted in the text. This information is available via the Internet at http://www.springer.com/chemistry/journal/11814.

REFERENCES

1. Z. Y. Chen, Y. Y He and H. W. Gao, *RSC Adv.*, **4**, 26309 (2014).
2. B. U. Yoo, M. H. Han, H. H. Nersisyan, J. H. Yoon, K. J. Lee and J. H. Lee, *Micropor. Mesopor. Mater.*, **190**, 139 (2014).
3. X. Cai, R. Y. Hong, L. S. Wang, X. Y. Wang, H. Z. Li, Y. Zheng and D. G. Wei, *Chem. Eng. J.*, **151**, 380 (2009).
4. K. Okada, A. Shimai, T. Takei, S. Hayashi, A. Yasumori and K. J. D. MacKenzie, *Micropor. Mesopor. Mater.*, **21**, 289 (1998).
5. J. L. Zhang, Z. M. Liu and B. X. Han, *Micropor. Mesopor. Mater.*, **87**, 10 (2005).
6. Q. Y. Yu, J. F. Hui, P. P. Wang, B. Xu, J. Zhuang and X. Wang, *Nanoscale*, **4**, 7114 (2012).
7. S. Shi, M. Wang, C. Chen, F. Lu, X. Zheng, J. Gaoa and J. Xu, *RSC Adv.*, **3**, 1158 (2013).
8. M. A. Lucchini, A. Testino, A. Kambolis, C. Proff and C. Ludwig, *Appl. Catal. B-environ.*, **182**, 94 (2016).
9. Y. Wan and D. Y. Zhao, *Chem. Rev.*, **107**, 2821 (2007).
10. Q. Y. Yu, P. P. Wang, S. Hu, J. F. Hui, J. Zhuang and X. Wang, *Langmuir*, **27**, 7185 (2011).
11. Y. Chen, H. R. Chen, L. M. Guo, Q. J. He, F. Chen, J. Zhou, J. W. Feng and J. L. Shi, *ACS Nano*, **4**, 529 (2010).
12. Y. Zhuang, Y. Yang, G. L. Xiang and X. Wang, *J. Phys. Chem. C*, **113**, 10441 (2009).
13. Y. Yang, Y. Zhuang, Y. H. He, B. Bai and X. Wang, *Nano Res.*, **3**, 581 (2010).
14. Y. Q. Wang, C. J. Tang, Q. Deng, C. H. Liang, D. H. L. Ng, F. L. Kwong, H. Q. Wang, W. P. Cai, L. D. Zhang and G. Z. Wang, *Langmuir*, **26**, 14830 (2010).
15. C. T. Kresge, M. E. Leonowicz, W. J. Roth, J. C. Vartuli and J. S. Beck, *Nature*, **359**, 710 (1992).
16. D. H. Pan, P. Yuan, L. Z. Zhao, N. Liu, L. Zhou, G. F. Wei, J. Zhang, Y. C. Ling, Y. Fan, B. Y. Wei, H. Y. Liu, C. Z. Yu and X. J. Bao, *Chem. Mater.*, **21**, 5413 (2009).
17. Y. Han, D. F. Li, L. Zhao, J. W. Song, X. Y. Yang, N. Li, Y. Di, C. J.

Li, S. Wu, X. Z. Xu, X. J. Meng, K. F. Lin and F. S. Xia, *Angew. Chem. Int. Ed.*, **42**, 3633 (2003).
18. A. Sayari, *Angew. Chem. Int. Ed.*, **39**, 2920 (2000).
19. A. F. Gross, V. H. Le, B. L. Kirsch, A. E. Riley and S. H. Tolbert, *Chem. Mater.*, **13**, 3571 (2001).
20. T. Martin, A. Galarneau, F. Di Renzo, F. Fajula and D. Plee, *Angew. Chem. Int. Ed.*, **41**, 2590 (2002).
21. A. Galarneau, J. Iapichella, K. Bonhomme, F. Di Renzo, P. Kooyman, O. Terasaki and F. Fajula, *Adv. Funct. Mater.*, **16**, 1657 (2006).
22. T. X. Zhao, B. Guo, L. M. Han, N. Zhu, F. Gao, Q. Li, L. H. Li and J. B. Zhang, *ChemPhysChem*, **16**, 2106 (2015).
23. T. X. Zhao, B. Guo, F. Zhang, F. Sha, Q. Li and J. B. Zhang, *ACS Appl. Mater. Interfaces*, **7**, 15918 (2015).
24. B. Guo, T. X. Zhao, F. Sha, F. Zhang, Q. Li and J. B. Zhang, *Korean J. Chem. Eng.*, **33**, 1883 (2016).
25. M. Grun, I. Lauer and K. K. Unger, *Adv. Mater.*, **9**, 254 (1997).
26. W. C. Yoo and A. Stein, *Chem. Mater.*, **23**, 1761 (2011).
27. G. Zhang, Y. Yu, X. Chen, Y. Han, Y. Di, B. Yang, F. Xiao and J. Shen, J. *Colloid Interface Sci.*, **63**, 467 (2003).
28. W. J. Tang, H. J. Huang, Y. J. Gao, X. Y. Liu, X. Y. Yang, H. J. Ni and J. B. Zhang, *Mater. Design*, **88**, 1191 (2015).
29. Y. J. Gao, H. J. Huang, W. J. Tang, X. Y. Liu, X. Y. Yang and J. B. Zhang, *Micropor. Mesopor. Mater.*, **217**, 210 (2015).
30. D. M. Nevskaia, E. Castillejos-Lopez, V. Munoz and A. Guerrero-Ruiz, *Environ. Sci. Technol.*, **38**, 5786 (2004).
31. J. Y. Hu, T. Aizawa and Y. Magara, *Water Res.*, **33**, 417 (1999).
32. A. Kortenkamp and R. Altenburger, *Sci. Total Environ.*, **233**, 131 (1999).
33. S. H. Song and M. Kang, *J. Ind. Eng. Chem.*, **14**, 785 (2008).
34. M. Jiang, Q. Wang, X. Jin and Z. Chen, *J. Hazard. Mater.*, **170**, 332 (2009).
35. T. A. Saleh and V. K. Gupta, *Adv. Colloid Interface Sci.*, **211**, 93 (2014).
36. M. M. Rao, D. Ramana, K. Seshaiah, M. Wang and S. Chien, *J. Hazard. Mater.*, **166**, 1006 (2009).
37. Y. H. Li, Q. J. Du, T. H. Liu, J. K. Sun, Y. Q. Jiao, Y. Z. Xia, L. H. Xia, Z. H. Wang, W. Zhang, K. L. Wang, H. W. Zhu and D. H. Wu, *Mater. Res. Bull.*, **47**, 1898 (2012).
38. Z. Y. Chen, Y. Y. He and H. W. Gao, *RSC Adv.*, **4**, 26309 (2014).
39. S. E. Lehman and S. C. Larsen, *Environ. Sci. Nano*, **1**, 200 (2014).
40. Y. Chang, J. B. Zhang, Q. Li, L. H. Li, B. Guo and T. X. Zhao, *Korean J. Chem. Eng.*, **31**, 2245 (2014).
41. J. G. Norwitz, A. H. Bardsley and P. N. Keliher, *Anal. Chim. Acta*, **128**, 251 (1981).
42. I. Langmuir, *J. Am. Chem. Soc.*, **40**, 1361 (1918).
43. L. Martinson, M. Alveteg and P. Warfvinge, *Environ. Pollut.*, **124**, 119 (2003).
44. R. S. Abolfazl, H. B. Ahmad, S. H. Hosseini, K. Kharghani, H. Zarei and A. Rastegar, *J. Hazard. Mater.*, **286**, 152 (2015).
45. M. Taghdiri, N. Zamani and S. A. Mousavian, *Desalin. Water. Treat.*, **56**, 3323 (2015).
46. T. Fan, Y. Liu, B. Feng, G. Zeng, C. Yang, M. Zhou, H. Zhou, Z. Tan and X.Wang, *J. Hazard. Mater.*, **160**, 655 (2008).
47. S. M. Tuzen, Ö. D. Uluözlü and M. Soylak, *Biochem. Chem. Eng. J.*, **37**, 151 (2007).
48. V. C. Srivastava, M. M. Swamy, I. D. Mall, B. Prasad and I. M. Mishra, *Colloids Surf., A.*, **272**, 89 (2006).
49. H. Tang, W. Zhou and L. Zhang, *J. Hazard. Mater.*, **209-210**, 218 (2012).
50. S. Onisei, Y. Pontikes, T. V. Gerven, G. N. Angelopoulos, T. Velea, V. Predica and P. Moldovan, *J. Hazard. Mater.*, **205-206**, 101 (2012).
51. A. Farrukh, F. Ashraf, A. Kaltbeitzel, X. Ling, M. Wagner, H. Duran, A. Ghaffar, H. U. Rehman, S. H. Parekh, K. F. Domke and B. Yameen, *Polym. Chem.*, **6**, 5782 (2015).
52. C. M. Huang, K. W. Cheng, G. T. Pan, W. S. Chang and T. K. Yang, *Chem. Eng. Sci.*, **65**, 148 (2010).
53. G. J. Yuan, J. B. Zhang, Y. F. Zhang, Y. N. Yan, X. X. Ju and J. M. Sun, *Korean J. Chem. Eng.*, **32**, 436 (2015).
54. L. T. Zhuravlev, *Colloid. Surf., A.*, **173**, 1 (2000).
55. Y. K. Buchman, E. Lellouche, S. Zigdon, M. Bechor, S. Michaeli and J. P. Lellouche, *Bioconjugate Chem.*, **24**, 2076 (2013).
56. B. D. Chen, L. Li, F. Tang and S. Qi, *Adv. Mater.*, **21**, 3804 (2009).
57. E. Reny, S. Yamanaka, C. Cros and M. Pouchard, *Chem. Commun.*, 2505 (2000).
58. X. M. Wang, X. Z. Du, C. L. Li and X. Cao, *Appl. Surf. Sci.*, **254**, 3753 (2008).
59. Z. Y. Chen, Y. Y. He and H. W. Gao, *RSC Adv.*, **4**, 26309 (2014).
60. N. Ghaemi, S. S. Madaeni, A. Alizadeh, H. Rajabi and P. Daraei, *J. Membr. Sci.*, **382**, 135 (2011).
61. J. Kim, S. J. Park and S. Kim, *J. Nanosci. Nanotechnol.*, **12**, 685 (2012).
62. P. Gupta, M. Kour, S. Paul and J. H. Clark, *RSC Adv.*, **4**, 7461 (2014).
63. M. Ghiaci, R. Kia, A. Abbaspur and F. Seyedeyn-Azad, *Sep. Purif. Technol.*, **40**, 285 (2004).
64. D. M. Zhang, Z. L. Chen, J. M. Shen and L. Yang, *Water Sci. Technol. W. Sup.*, **12**, 259 (2012).
65. J. G. Norwitz, A. H. Bardsley and P. N. Keliher, *Anal. Chim. Acta.*, **128**, 251 (1981).
66. B. Ozkaya, *J. Hazard. Mater.*, **B129**, 158 (2006).
67. X. X. Tao, G. Q. Zhou, X. P. Zhuang, B. W. Cheng, X. J. Li and H. J. Li, *RSC Adv.*, **5**, 5801 (2015).
68. L. J. Kennedy, J. J. Vijaya, G. Sekaran and K. Kayalvizhi, *J. Hazard. Mater.*, **149**, 134 (2007).
69. Y. H. Li, Q. J. Du, T. H. Liu, J. K. Sun, Y. Q. Jiao, Y. Z. Xia, L. H. Xia, Z. H. Wang, W. Zhang, K. L. Wang, H. W. Zhu and D. H. Wu, *Mater. Res. Bull.*, **47**, 1898 (2012).
70. B. Özkaya, *J. Hazard. Mater.*, **B 129**, 158 (2006).
71. R. Aravindhan, J. R. Rao and B. U. Nair, *J. Environ. Manage.*, **90**, 1877 (2009).
72. A. A. M. Daifullah and B. S. Girgis, *Water. Res.*, **32,** 1169 (1998).
73. B. J. Gao, P. F. Jiang, F. Q. An, S. Y. Zhao and Z. Ge, *Appl. Surf. Sci.*, **250,** 273 (2005).
74. M. Ahmaruzzaman and D. K. Sharma, *J. Colloid Interface Sci.*, **287**, 14 (2005).
75. H. L. Parkly, V. L. Budarin, J. H. Clark and A. J. Hunt, *ACS Sustainable Chem. Eng.*, **1**, 1311 (2013).
76. P. A. Mangrulkar, S. P. Kamble, J. Meshram and S. S. Rayalu, *J. Hazard. Mater.*, **160**, 414 (2008).
77. G. M. Forland and A. M. Blokhus, *J. Colloid Interface Sci.*, **310**, 431 (2007).
78. J. Toufaily, B. Koubaissy, L. Kafrouny, H. Hamad, P. Magnoux, L. Ghannam, A. Karout, H. Hazimeh, G. Nemra, M. Hamieh, N. Ajouz and T. Hamieh, *Cent. Eur. J. Eng.*, **3**, 126 (2013).

79. F. Kleitz,W. Schmidt and F. SchUth, *Micropor. Mesopor. Mater.*, **44**, 95 (2001).
80. L. Huang, Q. Huang, H. Xiao and M. Eic, *Micropor. Mesopor. Mater.*, **98**, 330 (2007).
81. T. M. Al-Bayati, *Particul Sci. Technol.*, **32**, 616 (2014).
82. P. Yu, Q. L. Sun, J. F. Li, Z. J. Tan, J. M. Pan and Y. S. Yan, *Korean J. Chem. Eng.*, **32**, 767 (2015).
83. M. A. Salam and R. C. Burk, *Water Air Soil Pollut.*, **210**, 101 (2010).
84. H. Tang, W. Zhou and L. Zhang, *J. Hazard. Mater.*, **209-210**, 218 (2012).

Supporting Information

A novel hydrothermal releasing synthesis of modified SiO_2 material and its application in phenol removal process

Xinyu Yang, Xiaoyao Liu, Wenjing Tang, Yajun Gao, Huijuan Ni, and Jianbin Zhang[†]

College of Chemical Engineering, Inner Mongolia University of Technology, Hohhot 010051, China
(*Received 3 May 2016 • accepted 2 November 2016*)

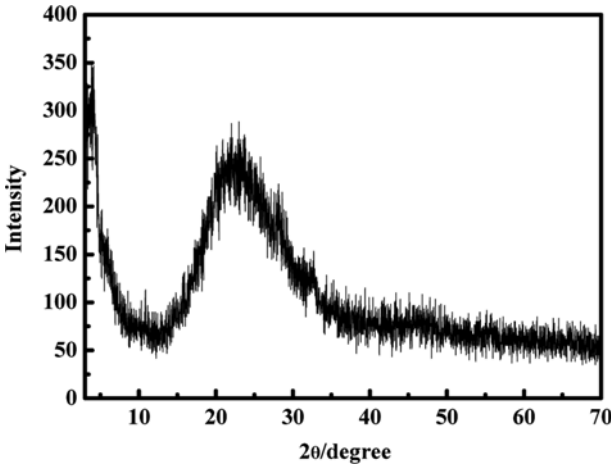

Fig. S1. XRD image of the SASM.